

# Influencing parameters on image quality using photon counting detectors for laminography

David SCHUMACHER<sup>1</sup>, Uwe EWERT<sup>1</sup>, Uwe ZSCHERPEL<sup>1</sup>

<sup>1</sup> Bundesanstalt für Materialforschung und -prüfung (BAM), Berlin, Germany

Contact e-mail: david.schumacher@bam.de

**Abstract.** Classical film radiography is a well-established NDT technique and it is most commonly used for testing weld seams and corroded pipes e.g. in oil and gas industry or in nuclear power plants. In the course of digitization, digital detector arrays (DDA) are finding their way into industrial applications and are replacing film radiography step by step. This study deals with the latest generation of DDAs, the photon counting and energy resolving detectors (PCD), and their characteristics compared to charge integrating detectors (CID). No matter which technology to use, radiography still lacks a general issue: A three-dimensional object is projected onto a two dimensional image. Of course, advanced computed tomography (CT) algorithms exist since many years, but if the object to investigate is too large to fit into the manipulation system or its shape is not appropriate, CT is not feasible or sensible to be applied. To overcome this limitation, numerous laminographic algorithms have been developed in the past. In this study, photon counting detectors are used in combination with co-planar translational laminography to gain reconstructed three-dimensional volumes. Both laminographic testing and PCDs require a serious knowledge of many parameters that can influence the image quality in the resulting datasets. These are e.g. the detector efficiency and calibration procedure, setting of energy thresholds, exposure data, number of projections, beam length correction and spatial resolution. The use of PCDs yields more variables to be considered compared to CIDs. The most important parameters in laminographic testing and in the use of PCDs are described in this study and limits are discussed.

## Introduction

The field of radiographic imaging is facing the challenges of the process of digitization as well as all other branches in industry and public life. Film radiography which is used in the non-destructive testing (NDT) since decades is being replaced by digital radiography based on imaging plates or digital detector arrays (DDA) step by step. DDAs offer higher contrast sensitivity compared to classical film radiography and allow the application of digital image processing (like filtering etc.) to enhance the representation of the results.

The latest generation of DDAs which came up in the last years is called photon counting detectors (PCD). The detecting principle is different from common charge integrating detectors (CID) which offers new opportunities e.g. regarding long term measurements and high wall thickness samples. Especially the high spatial resolution even under large angle of incidences (AOI) offer significant advantages compared to CIDs. [1, 2]

No matter which technique to use, DDAs in general allow the application of 3D reconstruction algorithms by which depth information is generated from hundreds or



thousands of single projection images. Numerous computed tomography (CT) algorithms exist since many years and have been well established in medicine and NDT applications. If depth information is needed to characterize or measure a defect in a component which is built-in stationary or too large to fit into a manipulation system, other techniques need to be applied. For those applications various laminography algorithms have been developed in the past, e.g. rotational laminography, swing laminography or translational laminography.

Besides the gain of depth information, the probability to hit a crack in a beneficial way (parallel to its extent in depth) and therefore to maximize the contrast, is being increased by the multiple projections acquired under various AOIs during a laminographic scan. If planning studies on the probability of detection (POD) dealing with laminographic investigations using PCDs, the knowledge of parameters which influence the result of the reconstructed dataset is essential to validate the reliability of this method (e.g. by conducting a multi-parameter PCD analysis like in [3]). This study aims at highlighting the most important parameters on the setup side (laminography and PCD) without taking the size, orientation etc. of the defect itself into account.

## **1. Principles**

### *1.1 Photon Counting Detectors*

Indirect detecting DDAs are commonly based on scintillation layers (e.g. CsI or Gd<sub>2</sub>O<sub>2</sub>S) which convert incident x-ray photons into visible light which is detected by underlying photo diodes (Figure 1). The amount of optical photons produced within the scintillation layer is strongly depending on the energy of the x-ray photon. A high energetic x-ray photon creates more optical photons than a low energetic one, i.e. the resulting signal is an integral of the charge created in the photo diodes by the total amount of the absorbed photons and their energy. Furthermore, the conversion process is associated with scattering of the optical photons. This generates an inner unsharpness which limits the achievable basic spatial resolution ( $SR_b$ ) and is always larger than the pixel size of the CID.

The difference in the signal generation process is described in Figure 1. Direct detecting detectors (like PCDs) do not have a scintillation layer in which optical rays are generated. The incident x-ray photons are directly converted into electron-hole pairs inside of a semi-conductor crystalline (e.g. made from Si or CdTe). [4, 5]

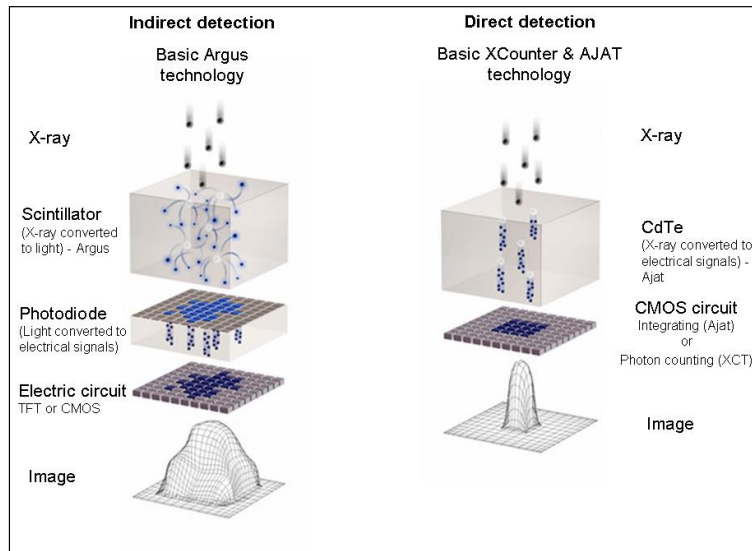


Figure 1: Comparison between indirect (left) and direct (right) detection of X-rays<sup>1</sup>

The semi-conductor detection layer is biased with a voltage of several hundred Volts which generates an electrical field across the crystalline in which the electron-hole pairs are accelerated towards the anode or cathode, respectively. An underlying CMOS circuit processes those directly generated electrical signals which create the resulting image. The absence of optical scattering leads to a much lower inner unsharpness ( $SR_b$  equals usually pixel size) and therefore much sharper images.

## 1.2 Laminography

The laminographic technique which is used in this study is called co-planar translational laminography because the x-ray tube fulfils a linear movement parallel to the horizontal pixel lines of the DDA. During this manipulation a sequence of projection images is acquired by the DDA where each projection image represents the sample(s) from a different angle of incidence (AOI). After acquisition, the stack of projection images is passed to a *weighted filtered shift-average* reconstruction algorithm [6] which delivers a three-dimensional dataset of the sample(s) or part of the sample which were investigated.

Figure 2a depicts the principle of a co-planar translational laminography and Figure 2b shows an example where this laminography technique was applied to investigate a vertical tail of an airplane made of CFRP [7].

<sup>1</sup> from: <http://directconversion.com/technology/>

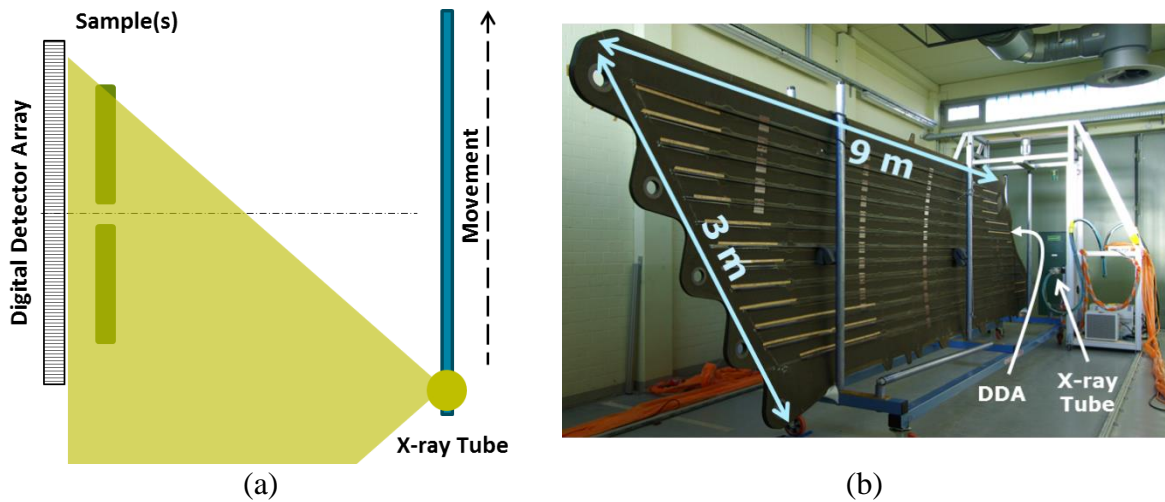


**Figure 2: Principle of co-planar translational laminography (a) and example setup for investigating a vertical tail made of CFRP of an airplane<sup>2</sup> (b)**

Figure 3 exemplarily shows a comparison between the results of a laminographic reconstruction of a CFRP stringer attached to a plate and a mechanical micro sectioning which was conducted to validate the results of the laminography. The laminographic reconstruction could find a crack at the right hand side of the stringer and its size and shape could be validated by micro sectioning [7].

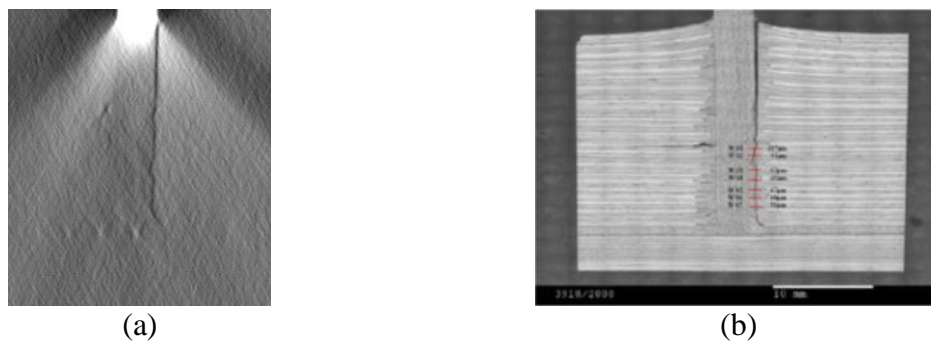


**Figure 3: Comparison between the results of co-planar translational laminography (a) and mechanical micro sectioning (b). Object of interest were CFRP components and the applied stringers to stiffen the structure. On the right hand side of the stringer, a crack was found by the laminographic investigation which could be validated by the micro sectioning<sup>2</sup>.**

## 2. Influencing Parameters

### 2.1 Photon Counting Detectors

PCDs in general require a more sensitive handling in terms of e.g. temperature stability and radiographic parameters than CIDs normally do. Especially the temperature of the sensitive detection layer and the exposure spectra can heavily influence the performance of a PCD.

Figure 4 illustrates the temperature influence during an investigation of a CFRP plate containing glass fiber wefts. In Figure 4a the temperature during the measurement is the same temperature which prevailed during the calibration process, therefore, a plain radiography is acquired. In Figure 4b the temperature changed between calibration process

<sup>2</sup> from: [7]

and measurement which results in a change of detector efficiency as a consequence of the temperature dependency of the carrier mobility and drift velocity, respectively [8, 9]. As in CIDs no charge carriers but photons are generated, this temperature effect can be observed primarily for PCDs in a highly distinct way.

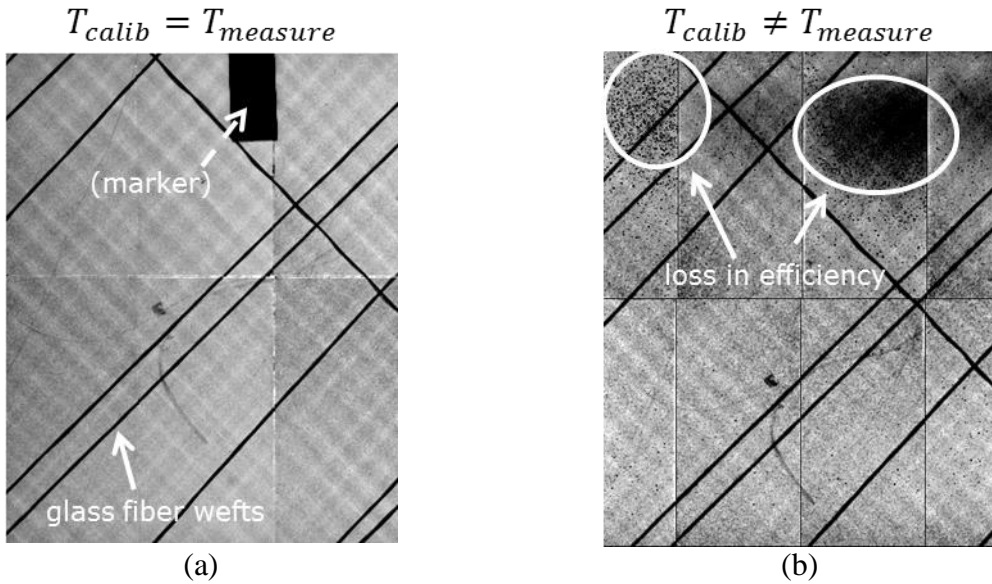


**Figure 4: A CFRP component containing glass fiber wefts was investigated using a PCD. Normal image with stable temperature (a) vs. instable temperature or temperature difference between measurement and calibration (b). In the latter case (b), dark spots/areas are distributed across the whole image which relate to a difference (here: loss) in efficiency due to temperature change.**

Besides the influence of the temperature, PCDs are very sensitive to the incident x-ray spectra. Figure 5 shows qualitatively three different spectra which have been used for calibration and measurement of the images shown in Figure 6. A detector calibration is generally done to compensate differences in pixel response to equal incident intensity. In case of PCDs, the spectrum of calibration and measurement needs to be identical to acquire high-quality images or at least reasonable images. Hence, the spectral response needs particular consideration for objects with large differences in penetration length, because the incident spectrum is hardened by the investigated object, as well.

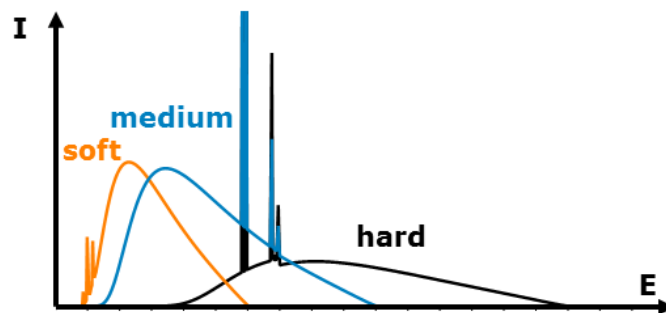


**Figure 5: Soft, medium and hard x-ray spectra (qualitatively).**

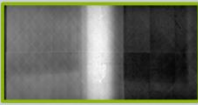
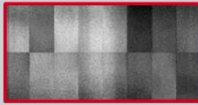
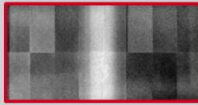
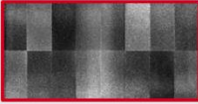
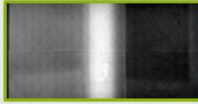
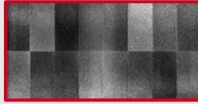
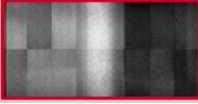
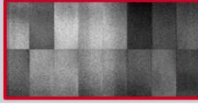
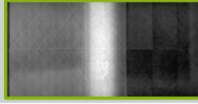
| Measurement spectrum → | hard  | medium   | soft  |
|------------------------|---|--|---|
| Calibration spectrum ↓ |   |  |   |
| hard                   |  |  |  |
| medium                 |  |  |  |
| soft                   |  |  |  |

Figure 6: Measurement vs. calibration spectra. Only if measurement and calibration spectra are identical, high-quality images can be acquired (green). In all other cases (red) the noise caused by the detector response corrupts the images.

## 2.2 Laminography

As the co-planar translational laminography intrinsically implies a limited view due to the limited AOIs, artefacts arise after reconstruction. The amount and intensity of those artefacts is mainly depending on the maximum AOI and the number of projection images acquired during the scan. Figure 7 shows different types of artefacts. Typical for laminographic applications are the cross artefacts (Figure 7a) which arise from the limited view and hence the incomplete dataset of laminographic reconstruction. Figure 7b represents a full dataset (CT) with sparse number of projections which result in star artefacts after reconstruction. The worst case, a combination of an incomplete dataset (like characteristic for laminography) and a sparse number of projections is shown in Figure 7c. In this case, the two small peaks left and right of the middle peak disappear within the noise of the artefacts. [10]

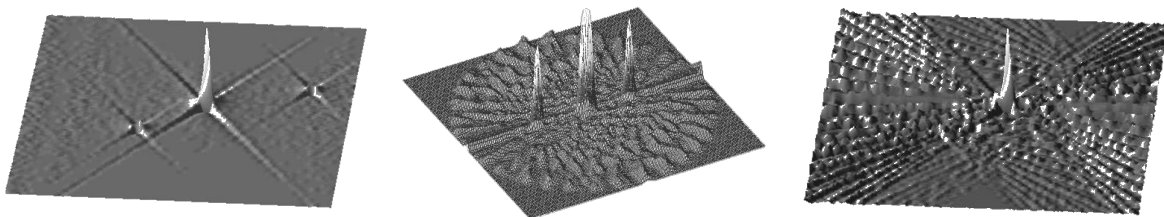
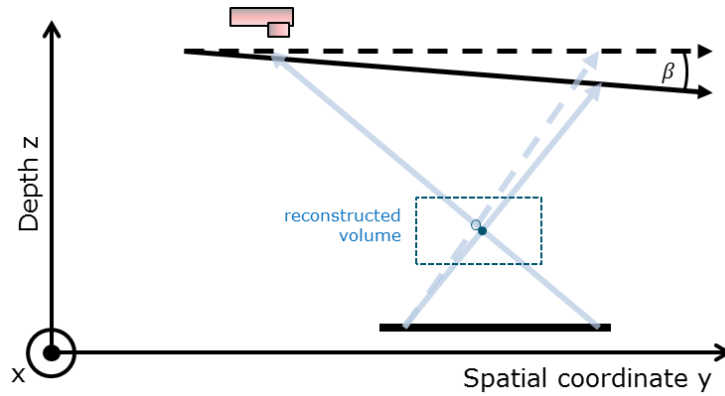


Figure 7: Types of artefacts occurring after reconstruction. Typical cross artefacts (a) after laminographic reconstruction as result of limited view (max. AOI). Star artefacts (b) arising from a sparse number of projection images but a full 360° dataset (CT). Superposition of cross and star artefacts (c) as a result of limited view and a low number of projections.<sup>3</sup>

The geometrical setup is an important point which influences the representation of any indications within the dataset. Especially an inclination of the manipulation axis towards the detector plane (Figure 8) results in a blurred shape of the indication (Figure 9).

<sup>3</sup> from: [10]



**Figure 8: Inclination of the manipulation axis towards the detector plane results in a blurred shape of the indication**

The rectangular indication is blurred to an arc-shape in case of a just slightly inclined manipulation axis. If the inclination is more than 1-dimensional (around x- and z-axis) the arc-shaped artefacts start to vary in shape and intensity depending on the displayed z-coordinate (depth).

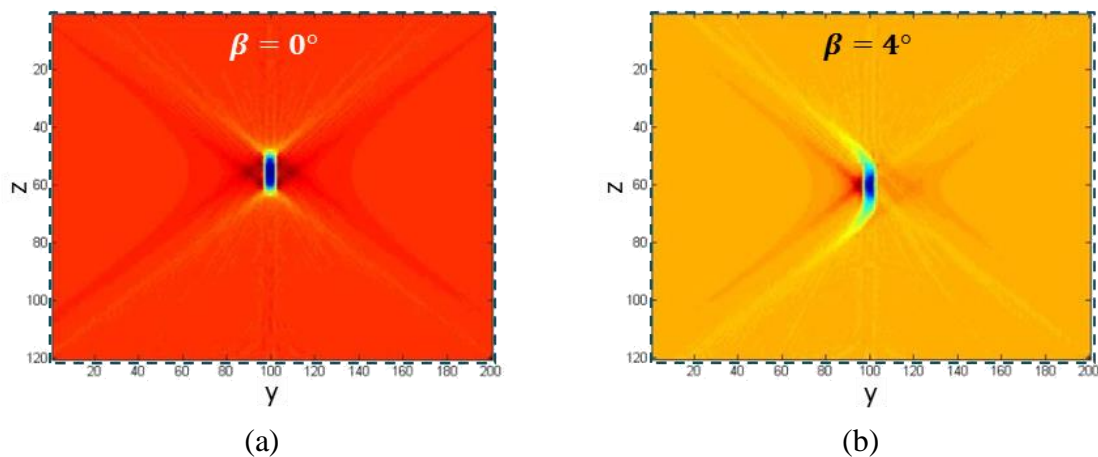


**Figure 9: Reconstructed volumes for different inclinations angles. At 0° inclination angle (a), the representation of the rectangular indication is as expected (incl. cross artefacts). Only a slightly inclined manipulation axis (b) results in an arc-shaped indication with a high intensity of cross artefacts.**

The drop in intensity under large AOIs is another major characteristic of laminographic applications. Due to higher penetration length and larger source-detector distance (SDD) the mean intensity in the projections images drops quickly with increasing AOIs (Figure 10, blue graph). Furthermore, due to equidistant step size on the manipulation axis, the angle difference between the outer projection images is smaller than between the central projections. This results in unevenly distributed amount of projections across the range of angles, i.e. few images in the middle, many images in the outer range (Figure 10, red graph). At an AOI of 40° the number of projections per angle is 1.7x higher than for an AOI of 0°.

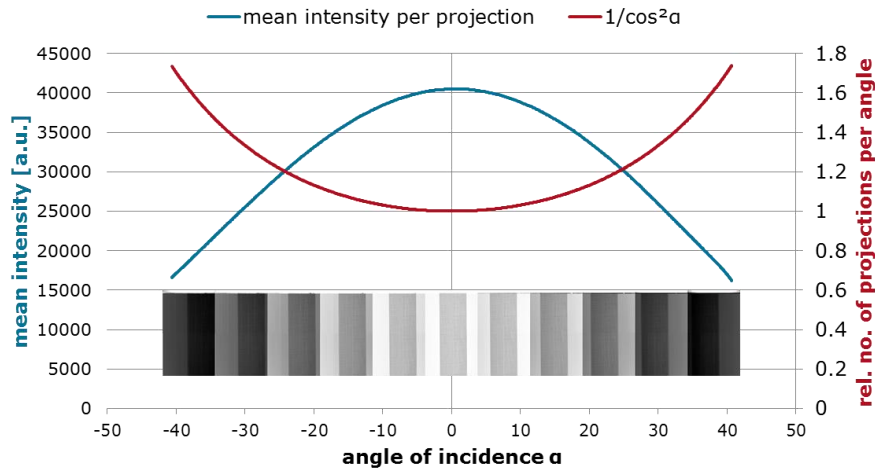


Figure 10: Mean intensity distribution of the projection images depending on the AOI (left, blue) and relative number of projections per angle for equidistant manipulation steps (right, red). Central projection ( $\alpha = 0^\circ$ ) equals 1. At  $\alpha = 40^\circ$  the number of projections per angle is 1.7x higher than for  $\alpha = 0^\circ$ .

### 3. Handling Requirements

#### 3.1 Photon Counting Detectors

The severe influence of temperature on the detector efficiency needs to be mitigated in case of PCDs by temperature stabilization. The simplest way to achieve passive temperature stabilization is to apply a high thermal capacity (e.g. copper plate) at the backside of the board. This stabilizes the temperature at least until the capacity is saturated. Another possibility is to attach an active cooling element (e.g. Peltier element and/or water cooling, Figure 11) to the board. This allows temperature stabilization within a range of  $\pm 0.1$  K. In case of Figure 11, the PCD is temperature controlled by a Peltier element which cools the backside of the board and transfers the heat to the detector case. From the detector case the heat is transferred by water cooling to a radiator which is cooled by air.

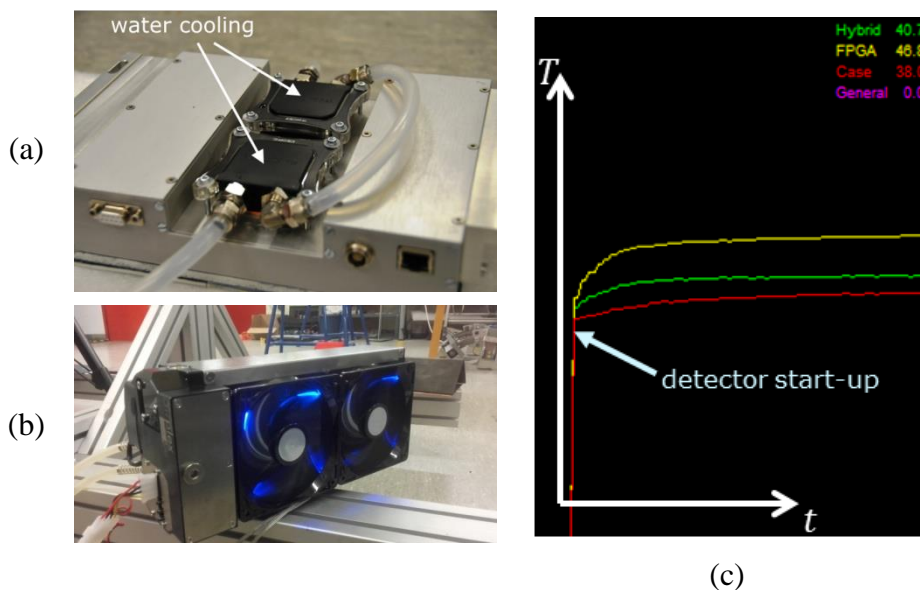
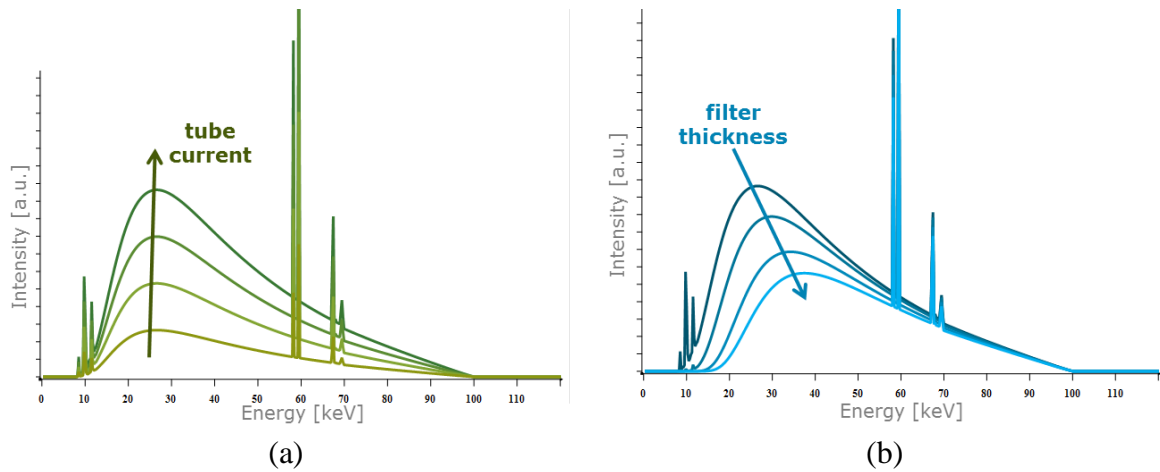


Figure 11: Water cooling attached to the back of a PCD (a) and the radiator (b). Temperature-over-time graph (c) at different sensors inside of a Peltier controlled PCD.

The spectral sensitivity of PCDs requires deeper consideration of the incident spectra. If the object to be investigated contains large differences in wall thickness and large steps in intensity are expected, a multi-gain calibration is required. A simple tube current (Figure 12a) calibration in which the difference in intensity is simulated by tuning the tube current works fine for most CID, because CIDs are not very sensitive to the incident spectra like PCDs are.

The incident spectrum is mainly influenced by the object to be investigated which implies the use of different filters during the multi-gain calibration to represent different material thicknesses (Figure 12b). This physically correct beam-hardening calibration method is mandatory for PCDs due to their spectral sensitivity. Of course, the beam-hardening calibration is valid and reasonable for CIDs, too.



**Figure 12: Influence of tube current (a) and filter thickness (i.e. beam-hardening; b) on the x-ray spectrum. Calibration using the tube current to manipulate the incident intensity works fine for most CIDs. Calibration using multiple pure filters of the material to be investigated is mandatory for PCDs and intrinsically the physically correct way to apply a calibration.**

### 3.2 Laminography

To limit the blurring of the indications due to any inclination of the manipulation axis, a proper geometric alignment of the setup is recommended. Moreover, to mitigate the influence of star artefacts arising from a sparse number of projections, a minimum number of projection images  $N_{im}$  is required depending on the setup (Figure 13 and Eq. 1).

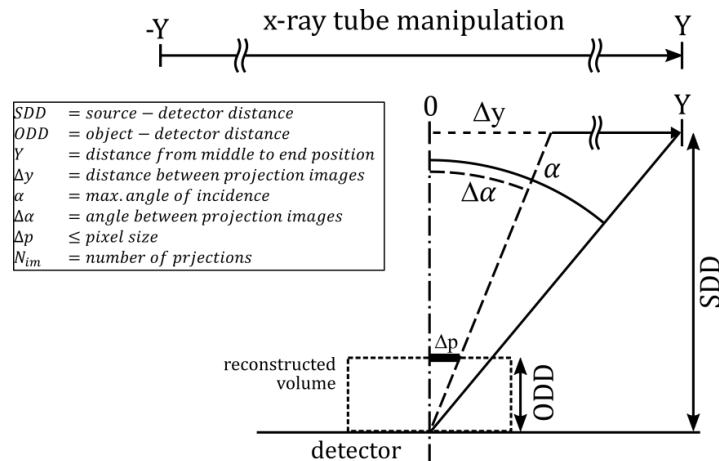


**Figure 13: Minimum number of projections  $N_{im}$  needed (for equidistant step size  $\Delta y$ ) to limit the maximum unsharpness of the reconstructed volume to be maximum pixel size  $\Delta p$ .**

$$N_{im} \geq \frac{2Y}{\Delta y} = \frac{2Y \cdot ODD}{\Delta p \cdot SDD} = \frac{2 \tan \alpha \cdot ODD}{\Delta p} \quad (1)$$

By only considering a proper geometric setup and a sufficient number of projection images, the typical cross artefacts arising from the limited view of the laminography cannot be overcome. But the representation of the cross artefacts can be mitigated by proper weighting the projection images. Figure 14 displays the influence of a  $\cos^2$ -weighting factor  $w_{\cos^2}$  and a Hamming window weighting factor  $w_{Hamming}$  on the representation of artefacts in a reconstructed sample dataset (cross section).

To suppress the influence of the increased noise level in the projections acquired under large AOIs, the projection images are each weighted by an individual weighting factor  $w_{\cos^2}$  (Eq. 2) depending on the geometric setup and therefore on the incident angle. Furthermore, an effective suppression of cross artefacts can be achieved by applying a weighting factor  $w_{Hamming}$  on each projection image using a Hamming window (defined in Eq. 3) depending on the distinct projection number.

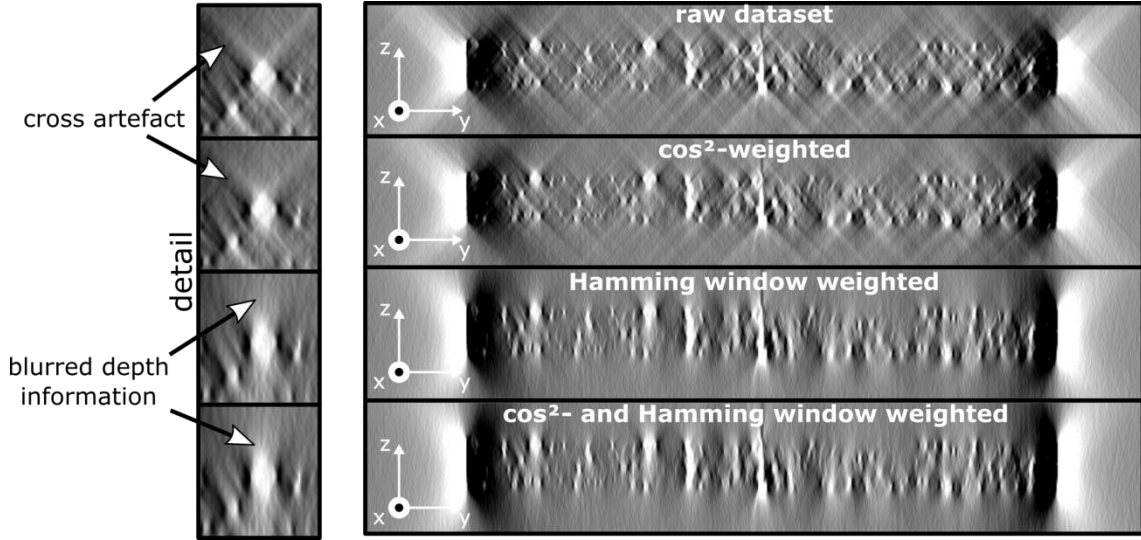


Figure 14: Digital cross sections of a sample dataset. Influence of  $\cos^2$ -weighting and Hamming window on the representation of reconstruction artefacts

$$w_{\cos^2} = \cos^2 \alpha = \frac{SDD^2}{SDD^2 + y^2} \quad (2)$$

$$w_{Hamming} = \frac{25}{46} + \frac{21}{46} \cos\left(\frac{2\pi i}{N_{im}-1}\right) \quad \text{with } i = 0 \dots (N_{im} - 1) \quad (3)$$

Both weighting factors decrease with increasing AOI. The advantage of suppressing the cross artefacts is traded for depth information. The outer projection images contribute most to the depth information and if they are weighted lower than the central projections during the reconstruction, depth information is blurred as shown in the detail images in Figure 14 on the left hand side.

## Conclusion

Although the properties of the defect itself are not considered in this study, they have a major impact on the outcome of a possible POD study. But it is not sufficient to consider only defect-related properties in order to evaluate a systems reliability. Therefore, this study illustrated important parameters which need to be respected when planning measurements and especially POD studies using laminographic trajectories and/or photon counting detectors. The result of a laminographic investigation is depending on many (mainly) geometric impacts and the algorithm of the reconstruction, as well. By manipulating the projection images during the reconstruction via smart weighting factors, the representation of artefacts and the depth resolution can be severely influenced. In case PCDs are used to acquire the projection images, especially the temperature and the incident spectra need to be considered in order to gain maximum quality results and a reasonable prediction of the systems reliability. Those parameters mentioned in this study could serve as input variables for multi-parameter POD studies.

## References

1. Walter D., Zscherpel U. (2015) *Properties and Application Areas of Photon Counting and Energy Resolving Digital Detector Arrays*. url: [http://www.ndt.net/events/DIR2015/app/content/Slides/92\\_Zscherpel.pdf](http://www.ndt.net/events/DIR2015/app/content/Slides/92_Zscherpel.pdf)
2. Walter D., Zscherpel U., Ewert U. (2016) *Photon Counting and Energy Discriminating X-Ray Detectors - Benefits and Applications*. url: <http://www.ndt.net/article/wcndt2016/papers/tu2b5.pdf>
3. Pavlovic M., Takahashi K., Muller C. (2012) *Probability of detection as a function of multiple influencing parameters*. Insight Non-Destructive Test. Cond. Monit. 54:606–611. doi: 10.1784/insi.2012.54.11.606
4. Taguchi K., Iwaczyk J.S. (2013) *Vision 20/20: Single photon counting x-ray detectors in medical imaging*. Med Phys. doi: <http://dx.doi.org/10.1118/1.4820371>
5. Ullberg C., Urech M., Weber N., et al. (2013) *Measurements of a Dual-Energy Fast Photon Counting CdTe Detector with Integrated Charge Sharing Correction*. Med Imaging 2013 Phys Med Imaging. doi: 10.1117/12.2007892
6. Andreas Deresch, Thiessenhusen K.-U., Ewert U., Bellon C. (2014) *Schneller Shift-Rekonstruktions-Algorithmus für die koplanare Translationslaminographie*. DGZfP Jahrestagung.
7. Ewert U., Redmer B., Rädcl C., et al. (2012) *Mobile Computed Tomography for Inspection of Large Stationary Components in Nuclear and Aerospace Industries*. Mater. Trans. 53:308–310. doi: 10.2320/matertrans.i-m2011848
8. Canali C., Martini M., Ottaviani G., Zanio K.R. (1971) *Transport Properties of CdTe*. Phys. Rev. B 4:422–431. doi: 10.1103/PhysRevB.4.422
9. Wolpert D., Ampadu P. (2012) *Managing temperature effects in nanoscale adaptive systems*. doi: 10.1007/978-1-4614-0748-5
10. Thiessenhusen K.-U., Ewert U., Redmer B., Bavendiek K. (2011) *Geometric Corrections in Coplanar Translational Laminography*. url: <http://www.ndt.net/article/dir2011/papers/we31.pdf>